JOURNAL OF RAMAN SPECTROSCOPY
J. Raman Spectrosc. 2007; **38**: 543–550
Published online 21 December 2006 in Wiley InterScience
(www.interscience.wiley.com) DOI: 10.1002/jrs.1677

JRS

Pulse shaping control of alignment dynamics in N_2

R. de Nalda,[1]* C. Horn,[2] M. Wollenhaupt,[2] M. Krug,[2] L. Bañares[3] and T. Baumert[2]

[1] Instituto de Química Física Rocasolano, CSIC, C/Serrano, 119, 28006 Madrid, Spain
[2] University of Kassel, Institute of Physics and Center for Interdisciplinary Nanostructure Science and Technology (CINSaT), Heinrich-Plett-Str. 40, D-34132 Kassel, Germany
[3] Departamento de Química Física, Facultad de Ciencias Químicas, Universidad Complutense de Madrid, 28040 Madrid, Spain

Received 30 August 2006; Accepted 17 November 2006

Control on the alignment transients of impulsively aligned ensembles of N_2 molecules has been demonstrated by the use of laser pulses shaped by a spatial light modulator. An alignment experiment has been inserted in the feedback loop of an evolutionary algorithm that found optimum pulse shapes for a set of criteria. Optimum pulse shapes for the maximization of total alignment and for the control of certain aspects of the revival structures are given. The physical mechanisms responsible for the control are analysed with the help of single-parameter control schemes and numerical simulations, which allowed us to explore the low-temperature region. This approach sheds light on the role played by different control mechanisms for the alignment dynamics of a molecular ensemble. Copyright © 2006 John Wiley & Sons, Ltd.

KEYWORDS: molecular alignment; coherent control; rotational revivals; pulse shaping; adaptive control

INTRODUCTION

Laser-induced alignment of ensembles of molecules in the gas phase has become a subject of great interest in the last decade.[1] The applications cover not only the more obvious ones concerning steric effects in reaction dynamics[2] and molecule–surface interactions, but also a subject like strong-field molecular physics is becoming very much entangled with the field of molecular alignment,[3,4] and even some of the first results in the emerging field of attosecond physics have been obtained in laser-aligned molecules.[5,6]

When a strong laser field interacts with a molecule that has an anisotropic polarizability (a linear molecule, for instance), an induced dipole is created that is in general not parallel to the electric field, and therefore interacts with the field producing a torque on the axes of the molecule.[7] This phenomenon permits obtaining narrow angular distributions in ensembles of gas-phase molecules and is known as *molecular alignment*.

In the temporal domain, two distinct regimes can be identified. In conditions where the duration of the laser pulse is long compared to the rotational period of the molecule, the situation is equivalent to the presence of a cw field. As the field is slowly turned on, the field-free states evolve adiabatically into pendular states,[7] and the only requirement for significant alignment to happen is that the Rabi coupling must be larger than the rotational energy of the molecular sample. The other extreme happens when the duration of the laser pulse is much shorter than the rotational period of the molecule. Raman excitation of rotational wave packets follows, and phasing and dephasing of their components in time create, in a manner analogous to rotational coherence spectroscopy,[8,9] rotational recurrences or 'revivals', where the molecular sample can recover a situation of high degree of alignment long after irradiation with the short pulse. The possibility to achieve this field-free alignment has made impulsive alignment, or, in general, non-adiabatic alignment, the preferred technique for most applications.

The phenomenon of non-adiabatic laser alignment of molecules has been studied in a number of experimental[10–14] and theoretical papers.[15–17] Most of the above have concentrated on the effects of a single Fourier transform-limited (FTL) laser pulse. In the past years, considerable effort has been devoted to studying the effect of two pulses,[18–21] and also of a train of pulses,[22–24] on molecular alignment. Poulsen *et al*.[25] have explored the possibilities of combining a short and a long laser pulse, finding an enhancement with respect to the degree of alignment that is attainable with each pulse separately. More recently, efforts have been directed to control non-adiabatic molecular alignment by using pulse shaping techniques.[20,26–28] In particular, Renard *et al*. have employed specific phase masks to create pulses that control the relative contribution of even and odd rotational states to the prepared rotational wave packet.[20,27] On the theoretical

*Correspondence to: R. de Nalda, Instituto de Química Física Rocasolano, CSIC, C/Serrano, 119, 28006 Madrid, Spain.
E-mail: r.nalda@iqfr.csic.es

side, the work by Salomon *et al*.[29] contains an approach for the optimization of molecular alignment by the use of arbitrary electric fields, but their algorithm finds an optimal field in the microwave region of the spectrum, not easily attainable with standard short-pulse lasers. Siedschlag *et al*.[30] studied numerically the efficiency of different evolutionary algorithms in optimizing total alignment by phase-shaping of the electric field under the constraint of a given maximum field intensity.

In this work we present a full account of our previous report,[28] in which we performed a general experimental exploration of pulse shaping in order to investigate to what extent it is possible to exert control on molecular alignment and on the dynamics of the rotational wave packets produced by a phase-shaped laser pulse. We have exploited the advantages of closed feedback loop procedures in combination with evolutionary algorithms[31–33] to explore a large parameter space of pulse shapes in search for laser pulses that maximized given effects. We have looked both for the optimization of the maximum degree of alignment attainable in a temporal window and the control of the temporal structure of rotational revivals. Numerical simulations were performed that agree well with our experimental findings at room temperature and that allow us to extend our investigation to lower temperatures. Results indicating that controllability is higher for higher temperatures are presented and discussed in terms of the relative roles played by coherent and incoherent effects on the alignment dynamics of a gas-phase molecular ensemble.

THEORY

For simplicity we are limiting the discussion here to the case relevant for our experiment, namely of homonuclear diatomic molecules interacting with a linearly polarized electric field. The Hamiltonian of the system then becomes:[7,13]

$$H_{\text{eff}} = B\mathbf{J}^2 - D\mathbf{J}^4 - \frac{1}{4}|\varepsilon(t)|^2\,\Delta\alpha\cos^2\theta \tag{1}$$

where B is the rotational constant, D is the centrifugal distortion constant, $\mathbf{J}$ is the angular momentum of the molecule, $\varepsilon\,(t)$ is the envelope function of the electric field, $\Delta\alpha = \alpha_{\parallel} - \alpha_{\perp}$ is the difference between the parallel and perpendicular components of the polarizability tensor of the molecule, and θ is the angle between the molecular axis and the polarization direction of the electric field. In writing Eqn (1) we left out a term that is independent of θ and thus does not affect the dynamics of the system. Furthermore, a rotating-wave-type approximation was employed[7] that eliminates the rapid oscillations due to the field amplitude.

The symmetry of Eqn (1) implies that dynamical alignment originates from Raman-type transitions, allowing only transitions with $\Delta M = 0$ and $\Delta J = \pm 2$. Starting from a pure rotational eigen state $|\psi_{J_0,M_0}(t=0)\rangle = |J_0, M_0\rangle$, for high enough field intensities a coherent rotational wave packet is created through successive ladder climbing. This can be written as:

$$|\psi_{J_0,M_0}(t)\rangle = \sum_{J\geq|M_0|} c_J^{J_0,M_0} \mathrm{e}^{-i(E_J t/\hbar)}|J, M_0\rangle \tag{2}$$

Here $E_J = B_0\ J(J+1) - D\ J^2\ (J+1)^2$ is the rotational energy of the sate $|J, M_0\rangle$, where we included the correction for the centrifugal distortion. The field-free states expansion coefficients $c_J^{J_0,M_0}$ are determined by the details of the laser–molecule interaction i.e. the temporal shape of the laser pulse.

The experimental observable corresponding to alignment is $\cos^2\theta$. In the case of an isotropic angular distribution $\langle\cos^2\theta\rangle = \frac{1}{3}$, while for the type of rotational wave packets discussed here $\langle\cos^2\theta\rangle_{J_0,M_0}(t) = \langle\psi_{J_0,M_0}(t)|\cos^2\theta|\psi_{J_0,M_0}(t)\rangle$ takes the form of beat structures oscillating rapidly with frequencies $\omega_J = (E_{J+2} - E_J)/\hbar$.

Owing to the low energy spacing of rotational levels, thermal ensemble averaging generally prevents experimental studies of the rotational dynamics of a pure state. Instead, the ensemble average $\langle\langle\cos^2\theta\rangle\rangle$ over the initial state distribution is observed. The time dependence of $\langle\langle\cos^2\theta\rangle\rangle(t)$ differs structurally from that of a pure state owing to the incoherent addition of the effects of the individual wave packets of the initial ensemble of rotational states. The fast oscillations cancel out, leaving non-vanishing alignment only at times of the so-called *revivals* occurring at integer (and fractional) multiples of the classical rotational period $T_{\text{R}} = \pi\hbar/B$.

For the simulations that were performed, we solved the time-dependent Schrödinger equation (Eqn (1)) numerically in the basis of field-free stationary rotational states $|J, M\rangle$ of the molecule to obtain the coefficients $c_J^{J_0,M_0}$ of Eqn (2). From the symmetry of $\cos^2\theta$ it follows that only the matrix elements

$$\langle J, M|\cos^2\theta|J, M\rangle = \frac{1}{3} + \frac{2}{3}\cdot\frac{J(J+1) - 3M^2}{(2J+3)(2J-1)} \tag{3}$$

$$\langle J, M|\cos^2\theta|J+2, M\rangle = \frac{\sqrt{(J-M+1)(J-M+2)}\ \sqrt{(J+M+1)(J+M+2)}}{(2J+3)\sqrt{(2J+1)(2J+5)}} \tag{4}$$

and $\langle J+2, M|\cos^2\theta|J, M\rangle = \langle J, M|\cos^2\theta|J+2, M\rangle$ of the Hamiltonian (Eqn (1)) are non-zero. As a consequence of this, the Hamiltonian decouples into systems of states having a fixed $M = M_0$ and only odd (even) J numbers. Numerically the evolution of the state vector was calculated by iteratively applying the short-time propagator $U(t + \Delta t, t) \approx \exp\left[-\frac{i}{\hbar}\boldsymbol{H}(t + \Delta t/2)\,\Delta t\right]$.

Finite temperature is considered by calculating the dynamics for a thermal ensemble of initial wave functions with a weight given by the Boltzmann factor and the multiplicity due to nuclear spin statistics.

DOI: 10.1002/jrs

The values of the molecular constants of N_2 we used for the simulations were $B_0 = 1.989581\,cm^{-1}$, $D = 5.76 \times 10^{-6}\,cm^{-1}$, and the polarizability anisotropy[34] $\Delta\alpha = 1.00\,Å^3$.

EXPERIMENTAL

Figure 1 gives a schematic representation of our experimental set-up. The laser system, comprising a Ti : sapphire oscillator and amplifier, produces pulses with a full width at half-maximum (FWHM) of 30 fs whose spectrum is centred at 790 nm. The alignment laser pulse passes through a pulse shaper[35,36] and is then focussed with a lens of $f = 10$ cm. The peak intensity in the focal region was adjusted to $I \sim 5 \times 10^{13}\,Wcm^{-2}$. In the interaction region the laser pulses induce alignment in N_2 and O_2 molecules from the air at room temperature.

For measuring the created alignment transients, a technique sensitive to the instantaneous birefringence of the media is used,[13,37] which measures the deviation from the isotropic case: $S \propto \left(\langle\langle\cos^2\theta\rangle\rangle - \frac{1}{3}\right)^2$. For that purpose, a delayed 395-nm laser pulse, whose polarization vector is at an angle of 45° with respect to that of the alignment pulse, probes the interaction region. The laser-induced birefringence in the molecular ensemble changes the polarization state of the probe laser by introducing some ellipticity after the interaction region. The beam is filtered through an analysing polarizer cube and the additional polarization component is detected by a photomultiplier. Experimental volume averaging was reduced by decreasing the probe diameter in the focal region with the help of a telescope, thereby probing only the inner part of the alignment distribution.

Figure 2(a) shows a typical result of the measurement of the transient birefringence created in air at room temperature by an unshaped alignment pulse. In the experimental trace, contributions from N_2 and O_2 are present, sometimes overlapping temporally. The lower panel, Fig. 2(c), shows the calculated values of $\langle\langle\cos^2\theta\rangle\rangle(t)$ for N_2. Large birefringence signals can be obtained in spite of the low values of $\langle\langle\cos^2\theta\rangle\rangle - \frac{1}{3}$ because of the large density–length product. The calculated values of $\langle\langle\cos^2\theta\rangle\rangle$ are then used to simulate the temporal behaviour of the (homodyned[13]) birefringence signal (Fig. 2(b)). For clarity, the effects of the convolution of the alignment signal with the probe pulse envelope were omitted in the theoretical calculations.

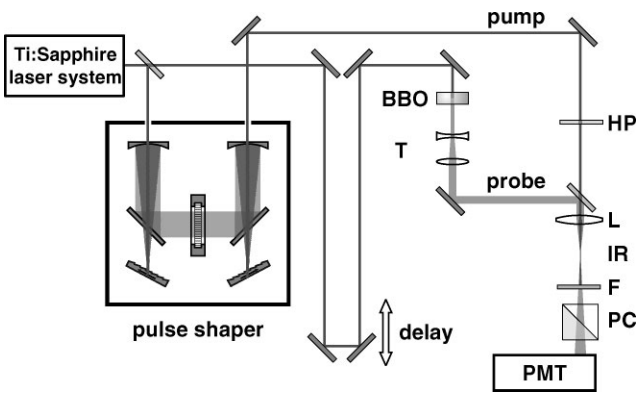

Figure 1. Experimental set-up. BBO: β-barium-borate second harmonic generation crystal; T: telescope (1 : 2); HP: Half-wave plate, rotates the pump polarization vector by 45°; L: focussing lens; IR: interaction region; F: filter to eliminate the pump laser; PC: polarizer cube; PMT: photomultiplier.

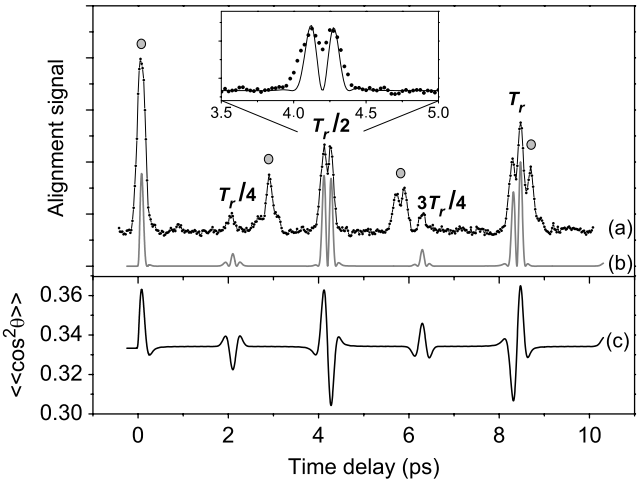

Figure 2. (a) Transient birefringence observed in atmosphere gases after flat-phase, short-pulse irradiation. The annotations $T_r/4$, $T_r/2$, $3T_r/4$, and T_r refer to submultiples of the rotational period (T_r) of the N_2 molecule. The grey circles indicate the temporal positions with a contribution from the O_2 molecule. (b) Simulated birefringence trace for N_2. (c) Calculated behaviour of $\langle\langle\cos^2\theta\rangle\rangle(t)$ in N_2 for a laser intensity of $I = 5 \times 10^{13}\,Wcm^{-2}$. The inset in the figure zooms in the area of the half revival ($T_r/2$) in N_2, which will be the chosen time window for this study.

The inset in Fig. 2 shows the temporal window where optimization procedures were applied in this work. The chosen region corresponds to the half revival in N_2, appearing at a time delay of $\tau \sim T_r/2 \sim 4.2$ ps, where T_r is the classical rotational period of the molecule. This area is favourable since there is no interference with O_2 signals. For an FTL pulse, the measured rotational half revival structure of N_2 consists of two peaks. The first peak, appearing at an earlier delay time, corresponds to the situation of alignment, where the inter-nuclear axes of the N_2 molecules are preferentially aligned parallel to the incident laser polarization. The second peak corresponds to anti-alignment (also called *planar delocalization*), where the molecules align preferentially in the plane perpendicular to the polarization vector of the laser. In the figure, both peaks appear with the same sign because homodyned detection[13] was employed.

In our experiments utilizing a closed feedback loop we used a GENITOR-type evolutionary algorithm[38] for optimization of the shape of the pump pulses, which was

DOI: 10.1002/jrs

applied on the parameters defining the phase masks in the Fourier plane. Different fitness functions were chosen for each case, as will be described below. In this scheme, we define an *individual* as a given phase mask. Starting with an initially random population of $N = 50$, in each evolution step one or two individuals were selected with a probability that increases exponentially with their fitness rank. From those individuals, a child was produced according to one of five different operators: uniform crossover, average, mutation, and two different creep operators. If the fitness of these new individuals is higher than that of the worst individuals in the population, they replace them. The choice of operator is random at the beginning, but successful operators are rewarded with higher probabilities along the progress of the evolution.

In practical terms, we found that it was advantageous to reduce the parameter space from the available 128 genes (which represent all the available pixels of the phase mask) to the first six terms of a Taylor expansion to describe the function applied in the phase mask. At the potential cost of finding less optimized solutions, this allows for a faster convergence that does not compromise the stability of the experiment over long periods of time. Fast convergence was a major factor in the experiment since, in order to determine the fitness function of each individual, it was necessary to do a short scan taking approximately 10 s. Typical runs evaluated a few hundred individuals.

RESULTS AND DISCUSSION

The first aim for optimization was the obvious: the search for the maximization of the total alignment signal. The temporal window of interest, corresponding to the first half revival of N_2, was scanned for each individual, and the fitness function was defined as the maximum signal found in the window. Note that by defining the fitness function this way, the algorithm was free to optimize only the alignment peak, only the anti-alignment peak or both. In practice, the best individuals turned out to be pretty symmetric, having approximately equal alignment and anti-alignment peak heights. Figure 3 shows the result of a typical run in the search for the strongest alignment. The original random populations, and even the best of their individuals, show an average fitness that is considerably lower than that obtained for unshaped FTL pulses (indicated by the grey band). Along the course of the evolution, the worst individuals disappear quickly from the population and, at a lower rate, new best individuals are found that tend to drag the overall quality of the population upwards. In the later stages of the evolution, the fitness of the best individual and the average fitness tend to converge. However, we found no conditions under which the fitness obtained at the end of an evolution procedure was higher than that obtained with the shortest pulse: FTL pulses produced the strongest alignment. This result is in accordance with evidence found by Renard *et al*.[20] We think

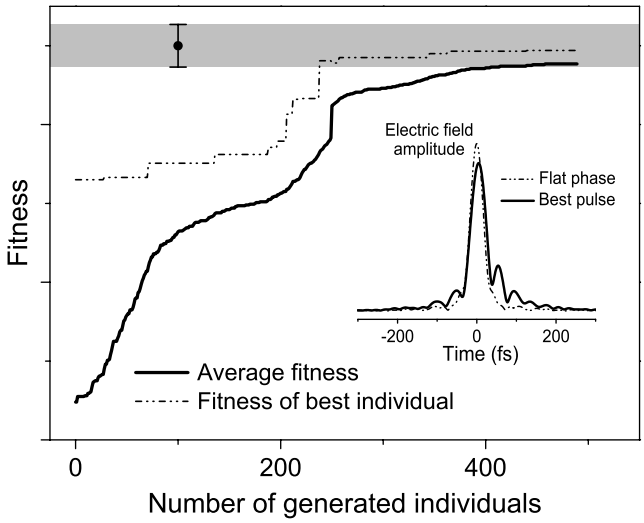

Figure 3. Feedback loop evolution of the fitness function (i.e. a measure of the degree of alignment) obtained for the half revival of N_2. The grey band indicates the error bar of the measured fitness for a spectrally unshaped pulse (flat-phase). See text for details of the evolution procedure. The inset shows the temporal structure of the best pulse (calculated from the pulse spectrum and the applied phase) in comparison with an unshaped pulse.

that this finding is quite general because the parameter space explored by our evolutionary algorithm, although limited, is clearly more extensive than that of any single-parameter control scheme. On the other hand, it is clear that these findings are valid only in the regime studied here, in which ionization does not play a significant role even for the shortest pulses possible. If the available pulse intensity is high enough so that ionization is important, it has been shown that pulse pairs can overcome the limit set by the onset of ionization.[19,21,25,30]

In the second part of our experiment, the goal was to control the temporal shape of a revival structure. We chose the fitness function as the ratio between the alignment peak and the anti-alignment peak in the same region of the transient as before. Fitness for unshaped pulses was approximately equal to unity, corresponding to a situation in which the intensity of the alignment and the anti-alignment peaks is the same. Given this objective, the evolutionary procedure did find individuals whose fitness function was significantly higher than that of unshaped pulses, that is, pulses that induced strong alignment but weak anti-alignment in the half revival of N_2. Likewise, the opposite result – higher anti-alignment than alignment – could be achieved by redefining the fitness function accordingly. Analysis of the best individuals after an evolutionary run showed that the key feature in the optimization was the temporal envelope of the field rather than the details of the phase function applied. Figure 4 shows the transients produced by the best individuals for each fitness function,

DOI: 10.1002/jrs

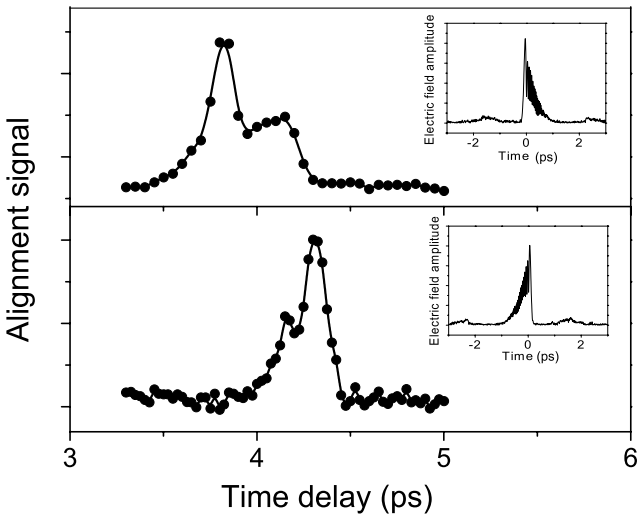

Figure 4. Demonstration of control on the temporal structure of alignment revivals with a closed-loop evolutionary algorithm. Alignment transients for the first half revival of N_2 that correspond to the best individuals of corresponding evolutionary runs. (a) Optimization of alignment (*vs*) anti-alignment. (b) Optimization of anti-alignment (*vs*) alignment. The curves are intended as visual guides. The insets show pulse shapes of representative good individuals for the maximization of alignment (*vs*) anti-alignment or vice versa.

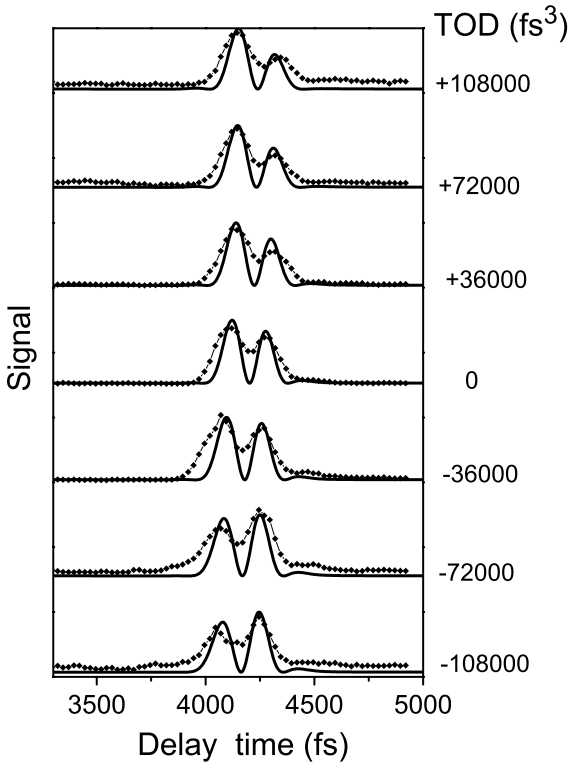

Figure 5. Experiment and simulation showing one-parameter control on the relative magnitude of the alignment and anti-alignment peaks in the first half revival of N_2 by applying pulses with third-order dispersion (TOD). TOD values are scanned from $-108\,000$ to $+108\,000$ fs^3 in steps of 36 000 fs^3 from the lower trace to the top trace. Pulses with positive TOD produce enhancement in the ratio of the alignment to the anti-alignment peak. The opposite is true for pulses with negative TOD. Since the total alignment decreases for increasing TOD owing to the lower pulse intensity (the total signal for a TOD phase of $+108\,000$ fs^3 drops by a factor of about 7 compared to an FTL pulse) the experimental traces are normalized for better comparability, and each theoretical curve *y*-scaled to fit the experiment.

together with typical pulse shapes that produced each effect. As the examples of the figure show, it was a consistent feature for pulses that maximized the alignment (*vs*) anti-alignment ratio to have a steep leading edge and a slow trailing edge. Pulses that achieved the opposite effect (higher anti-alignment to alignment ratio) were the temporal mirror images of the former. Optical gating techniques[39] were employed to verify the pulse shapes for some of the best individuals in order to check the experimental pulse form.

The fact that control of the structure of the revivals had been achieved simply by an asymmetry in the temporal shape of the pulses led us towards the search for a single-parameter control scheme, which could then be a first step to get a clearer picture of the underlying physical mechanism responsible for controllability. The lowest order coefficient in a polynomial expansion of the phase function to produce asymmetric pulse shapes is the one that corresponds to third-order dispersion (TOD) and was therefore chosen as parameter for a systematic study of its effect on the revival structure in N_2. The TOD coefficient was scanned from $-108\,000$ fs^3 to $+108\,000$ fs^3 in steps of 36 000 fs^3, and the alignment transient was measured for each condition. The results are shown in Fig. 5 together with numerical simulations. As can be seen, the same type of temporal shape asymmetry in the pulse produces the same effect on the alignment transient as was found through the evolutionary algorithm: sharp leading edge and slow trailing edge leading to a higher alignment to anti-alignment ratio and vice versa.

Comparing the experimental data to the simulation results in Fig. 5, an excellent agreement was found, which added to the demonstration that control on the asymmetry of the temporal shape of the laser pulse provides substantial control of the relative strength of alignment and anti-alignment.

Our experiment was carried out at room temperature and it is an important question how this influenced the possibility of controlling the alignment transients. Temperature is a crucial parameter in laser-induced molecular alignment since it determines the number of rotational levels that are populated in the thermal ensemble before laser excitation. The revival structures themselves are an effect of thermal averaging and the maximum degree of alignment decreases significantly with increasing temperature. Being

DOI: 10.1002/jrs

restricted to room temperature implies that the initial rotational distributions are broad, the degree of alignment is relatively low, and the alignment revivals are narrow in time.[40,41]

To address the question of the temperature dependence of the control scheme, we extended our numerical simulations to explore temperature regimes not investigated by our experiment. We have concentrated on the ability of TOD to control the anti-alignment to alignment ratio in the first half revival of N_2. In the top section of Fig. 6 (panels (a)) alignment transients are shown that are calculated at three different temperatures for pulses with positive (top row) or negative (bottom row) TOD of 120 000 fs^3. The stronger values for alignment and the temporally broader alignment structures obtained with low temperatures are in agreement with previous studies.[40] On all the transients displayed, the first peak in time corresponds to alignment, and the second to anti-alignment. Figure 6(b) shows the results of the systematic study performed for a whole range of temperatures between 1 and 500 K. The symbols (open or filled) indicate the ratio r_+ or (r_-) between the anti-alignment and the alignment peaks for positive (negative) TOD. For comparison, we also show the ratios r_0 that result from a transform-limited pulse (the corresponding transients are not shown in Fig. 6(a)). To get an understanding of the effect of the temperature on the controllability, we have to first discuss the temperature effects on the FTL – pulse ratio r_0. In accordance with our experimental results discussed above (Fig. 2), the ratio r_0 is approximately equal to 1 at room temperature. As Fig. 6(b) shows, the situation is different for lower temperatures. The ratio decreases, meaning that the alignment peak is favoured as temperature gets lower. A clear contribution to this is the phenomenon of 'incoherent alignment',[12] an effect which is more pronounced for lower temperatures and which shifts the time-independent baseline of the alignment transient to a value higher than the isotropic value of 1/3, thereby favouring alignment over anti-alignment. When looking at the difference between r_+, r_0, and r_- in Fig. 6(b), it is clear that no control is possible through the application of a TOD phase for very low temperatures, which can also be seen in the negligible difference that is obtained in the transients of panels in Fig. 6(a) for $T = 3$ K. As the temperature is increased, the effect of the TOD phase increases, while at the same time the biasing effect of the 'incoherent alignment' vanishes. For positive TOD of +120 000 fs^3, both effects just compensate, leaving the ratio almost constant. On the other hand, both effects add up in the case of negative TOD, leading to transients in which the anti-alignment dominates for $T > 100$ K. For room temperature, the calculations once again are in agreement with our experimental results, showing that one can switch to alignment (anti-alignment) dominated transients by applying a positive (negative) TOD phase.

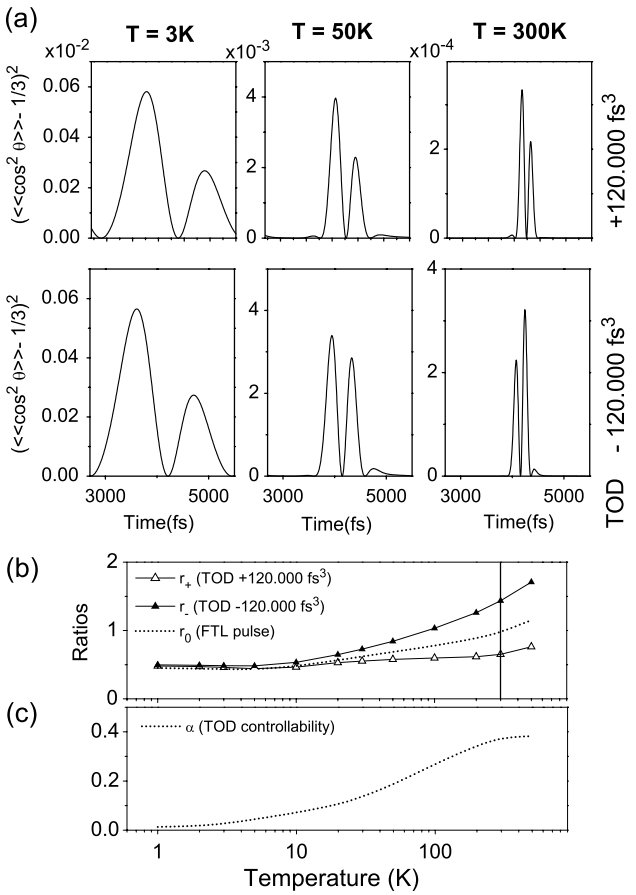

Figure 6. Simulation of the TOD control on the enhancement of anti-alignment (*vs*) alignment (and vice versa) as a function of temperature. The simulated intensity (of the corresponding FTL pulse) was 5×10^{13} Wcm^{-2}. (a) Simulated alignment transients of the first half revival in N_2 for different temperatures. The top row corresponds to the application of pulses with a positive TOD of +120 000 fs^3, the second row, to a negative TOD of −120 000 fs^3. (b) Ratio r of anti-alignment to alignment peak heights. Open symbols (△): r_+ ratio for a positive TOD of +120 000 fs^3. Filled symbols (▲): r_- ratio for a negative TOD of −120 000 fs^3. Dashed line: ratio r_0 for a transform-limited pulse shown for comparison. The vertical line at 300 K indicates the temperature at which the experiments of this work were performed. (c) TOD controllability $\alpha = (r_- - r_+)/(r_- + r_+)$ giving a measure of controllability as a function of temperature: a value of $\alpha = 1$ indicates perfect control; for $\alpha = 0$ no control is possible.

In Fig. 6(c), a parameter α is plotted, which is calculated as the contrast $\alpha = (r_- - r_+)/(r_- + r_+)$ that can be achieved at a given temperature and is meant to represent the controllability that is possible through the application of TOD phase. It is clear from the figure that for low temperatures control is negligible. Only for finite temperatures above ~50 K the application of TOD produces a significant modification on the structure of the revival.

DOI: 10.1002/jrs

The finding that controllability is high for high temperatures and disappears for lower temperatures is somewhat counter-intuitive. One could assume that the large role played by incoherent addition of the effects of many different rotational wave packets at high temperature would erase the effects of pulse shaping on an individual wave packet. Thus, our results indicate that control is performed on the details of this incoherent addition of the ensemble, rather than on the excitation dynamics of each rotational state. Within this context, control of the anti-alignment (*vs*) alignment ratio with TOD is achieved by shifting in time the transients $\langle\cos^2\theta\rangle_{J_0,M_0}(t)$ of the different components of the thermal ensemble, resulting in a different net alignment $\langle\langle\cos^2\theta\rangle\rangle(t)$ through either an effective cancellation or an enhancement at a specific time resulting in different temporal shapes of the revival structure.

More work needs to be done to obtain a full understanding of the mechanisms that are responsible for the demonstrated control of the alignment transients. Moreover, it still has to be seen to what extent one can control the shape of the alignment transient at will. Interesting applications include exploiting the controllability of revival structures for the control of the rapidly varying refractive index that can lead to self-phase modulation[42] and exploring the possibility of enhancing overall alignment in more complex molecules. Polarization shaping[43] should be highly beneficial in the optimization of 3D alignment of asymmetric tops.[44] The method shown recently[45] for the single-shot measurement of revival structures would be particularly suitable for a further exploration of the possibilities offered by pulse shaping techniques for the control of molecular alignment in the impulsive regime.

CONCLUSIONS

In conclusion, we have shown that the alignment transients that appear after short-pulse irradiation of gas-phase molecules can be controlled by applying tailored laser pulses. An evolutionary method has proven successful in the optimization of a given desired feature of the alignment transient and it has provided clues for single-parameter control schemes. After a significant exploration of the parameter space by the evolutionary method, it has been found that overall molecular alignment is maximized for transform-limited pulses. Numerical simulations have allowed us to extend this work to lower temperatures. The finding that controllability is favoured by higher temperatures and vanishes completely as T approaches zero, meaning that it requires a broad initial J level distribution, indicates that this type of control is exerted on the ensemble effects rather than the coherent dynamics from each rotational state.

Acknowledgements

This work was supported by the Spanish–German project Acciones Integradas HA2003-0047. RdN and LB acknowledge financial support from the Spanish MEC through grant number CTQ2005-08493-C02-01.

REFERENCES

1. Stapelfeldt H, Seideman T. *Rev. Mod. Phys.* 2003; **75**: 543.
2. Larsen JJ, Wendt-Larsen I, Stapelfeldt H. *Phys. Rev. Lett.* 1999; **83**: 1123.
3. de Nalda R, Heesel E, Lein M, Hay N, Velotta R, Springate E, Castillejo M, Marangos JP. *Phys. Rev., A* 2004; **69**: 031804(R).
4. Kanai T, Minemoto S, Sakai H. *Nature* 2005; **435**: 470.
5. Itatani J, Levesque J, Zeidler D, Niikura H, Pepin H, Kieffer JC, Corkum PB, Villeneuve DM. *Nature* 2004; **432**: 867.
6. Zeidler D, Staudte A, Bardon AB, Villeneuve DM, Dörner R, Corkum PB. *Phys. Rev. Lett.* 2005; **95**: 203003.
7. Friedrich B, Herschbach D. *Phys. Rev. Lett.* 1995; **74**: 4623.
8. Felker PM. *J. Phys. Chem.* 1992; **96**: 7844.
9. Felker PM, Zewail AH. *Femtosecond Chemistry*, Manz J, Wöste L (eds). VCH Publishers, Inc.: New York, 1994; 193.
10. Rosca-Pruna F, Vrakking MJJ. *Phys. Rev. Lett.* 2001; **87**: 153902.
11. Rosca-Pruna F, Vrakking MJJ. *J. Chem. Phys.* 2002; **116**: 6567.
12. Dooley PW, Litvinyuk IV, Lee KF, Rayner DM, Spanner M, Villeneuve DM, Corkum PB. *Phys. Rev., A* 2003; **68**: 023406.
13. Renard V, Renard M, Guérin S, Pashayan YT, Lavorel B, Faucher O, Jauslin HR. *Phys. Rev. Lett.* 2003; **90**: 153601.
14. Hamilton E, Seideman T, Ejdrup T, Poulsen MD, Bisgaard CZ, Viftrup SS, Stapelfeldt H. *Phys. Rev., A* 2005; **72**: 043402.
15. Seideman T. *J. Chem. Phys.* 1995; **103**: 7887.
16. Ortigoso J, Rodríguez M, Gupta M, Friedrich B. *J. Chem. Phys.* 1999; **110**: 3870.
17. Torres R, de Nalda R, Marangos JP. *Phys. Rev., A* 2005; **72**: 023420.
18. Lee KF, Litvinyuk IV, Dooley PW, Spanner M, Villeneuve DM, Corkum PB. *J. Phys. B* 2004; **37**: L43.
19. Bisgaard CZ, Poulsen MD, Péronne E, Viftrup SS, Stapelfeldt H. *Phys. Rev. Lett.* 2004; **92**: 173004.
20. Renard M, Hertz E, Guérin S, Jauslin HR, Lavorel B, Faucher O. *Phys. Rev., A* 2005; **72**: 025401.
21. Bisgaard CZ, Viftrup SS, Stapelfeldt H. *Phys. Rev., A* 2006; **73**: 053410.
22. Leibscher M, Averbukh ISh, Rabitz H. *Phys. Rev. Lett.* 2003; **90**: 213001.
23. Spanner M, Shapiro EA, Ivanov M. *Phys. Rev. Lett.* 2004; **92**: 093001.
24. Stavros VG, Harel E, Leone SR. *J. Chem. Phys.* 2005; **122**: 064301.
25. Poulsen MD, Ejdrup T, Stapelfeldt H, Hamilton E, Seideman T. *Phys. Rev., A* 2006; **73**: 033405.
26. Underwood JG, Spanner M, Ivanov MY, Mottershead J, Sussman BJ, Stolow A. *Phys. Rev. Lett.* 2003; **90**: 223001.
27. Renard M, Hertz E, Lavorel B, Faucher O. *Phys. Rev., A* 2004; **69**: 043401.
28. Horn C, Wollenhaupt M, Krug M, Baumert T, de Nalda R, Bañares L. *Phys. Rev., A* 2006; **73**: 031401(R).
29. Salomon J, Dion CM, Turinici G. *J. Chem. Phys.* 2005; **123**: 144310.
30. Siedschlag Ch, Shir OM, Bäck Th, Vrakking MJJ. *Opt. Commun.* 2006; **264**: 511.
31. Judson RS, Rabitz H. *Phys. Rev. Lett.* 1992; **68**: 1500.
32. Assion A, Baumert T, Bergt M, Brixner T, Kiefer B, Seyfried V, Strehle M, Gerber G. *Science* 1998; **282**: 919.
33. Rabitz H, de Vivie-Riedle R, Motzkus M, Kompa K. *Science* 2000; **288**: 824.
34. Miller K. *J. Am. Chem. Soc.* 1990; **112**: 8543.
35. Weiner AM. *Rev. Sci. Instrum.* 2000; **71**: 1929.

36. Präkelt A, Wollenhaupt M, Assion A, Horn Ch, Sarpe-Tudoran C, Winter M, Baumert T. *Rev. Sci. Instrum.* 2003; **74**: 4950.
37. Heritage JP, Gustafson TK, Lin CH. *Phys. Rev. Lett.* 1975; **34**: 1299.
38. Whitley LD. *Proceedings of the 3rd International Conference on Genetic Algorithms*, Schaffer JD (ed.). George Mason University: San Mateo, CA, 1991; 116.
39. O'Shea P, Kimmel M, Gu X, Treblino R. *Opt. Lett.* 2001; **26**: 932.
40. Rosca-Pruna F, Vrakking MJJ. *J. Chem. Phys.* 2002; **116**: 6579.
41. Comstock M, Lozovoy VV, Dantus M. *Chem. Phys. Lett.* 2003; **372**: 739.
42. Bartels RA, Weinacht TC, Wagner N, Baertschy M, Greene CH, Murnane MM, Kapteyn HC. *Phys. Rev. Lett.* 2002; **88**: 013903.
43. Brixner T, Krampert G, Pfeifer T, Selle R, Gerber G, Wollenhaupt M, Graefe O, Horn C, Liese D, Baumert T. *Phys. Rev. Lett.* 2004; **92**: 208301.
44. Rouzée A, Guérin S, Boudon V, Lavorel B, Faucher O. *Phys. Rev., A* 2006; **73**: 033418.
45. Zamith S, Ansart Z, Lepine F, Vrakking MJJ. *Opt. Lett.* 2005; **30**: 2326.

DOI: 10.1002/jrs